An evaluation of lattice Boltzmann equation methods for simulating flow through porous media

C. Pan^a, L.-S. Luo^b, and C. T. Miller^a

^aCenter for the Advanced Study of the Environment Department of Environmental Sciences and Engineering, Box 7400 University of North Carolina, Chapel Hill, NC 27566-7400, USA

^bNational Institute of Aerospace, 144 Research Drive, Hampton, VA 23666, USA

We evaluated lattice Boltzmann equation (LBE) methods for modeling flow through porous media. We compared a three-dimensional, 19-velocity, multiple-relaxation-time (MRT) LBE model with a popular single-relaxation-time, Bhatnagar-Gross-Krook (BGK) LBE model. It can be shown that the latter (BGK-LBE) model is a spacial case of the former (MRT-LBE) model for a certain set of parameter constraints used in the collision operator. We compared the accuracy of the two models for two test cases: (1) Poiseuille flow between parallel plates, and (2) flow past a periodic simple cubic (SC) array of spheres. We also compared two solid-phase, boundary condition approximations: (1) a linearly interpolated bounce-back (LIBB) method, and (2) a standard bounce-back (SBB) method without interpolation. Our results clearly demonstrate advantages of the MRT-LBE model over its BGK counterpart, and the benefits of the LIBB method over the SBB method in terms of numerical accuracy.

1. INTRODUCTION

The lattice Boltzmann equation (LBE) method for modeling hydrodynamics [20] originated as an extension based upon the lattice-gas cellular automata method [7]. However, the LBE method can also be derived directly from the Boltzmann equation [11, 12]. This not only sets the LBE method on the solid foundation of classical kinetic theory, but also makes the LBE method amenable to numerical analysis. The LBE method has been proven to be equivalent to an explicit, first-order in time, second-order in space finite difference approximation of the incompressible Navier-Stokes equations [14, 16]. Thus, the LBE method can be viewed as a discrete approximation to the incompressible Navier Stokes equations, which is strongly based in a reduced kinetic theory applicable for modeling hydrodynamics [15].

The LBE method is gaining popularity in recent years because of its numerical accuracy, computational efficiency, intrinsic parallelism, and programming simplicity [4, 24]. Due to its kinetic origin, the LBE method has some features significantly different from conventional computational fluid dynamics methods based on a direct discretization of the Navier-Stokes equations. The LBE method evolves single-mass particle distribution

functions in phase space, instead of the macroscopic variables, such as fluid density ρ , flow velocity u, and temperature T. Consequently the boundary conditions in the LBE method are also expressed for the distribution functions rather than the flow variables commonly observed and controlled experimentally. While this aspect of the LBE method is often a source of confusion and criticism, boundary conditions in the LBE method can be equated to macroscopic hydrodynamic variables and rigorously analyzed [8–10, 13].

The LBE method has proven especially useful for simulating flow in porous media, which has been well documented in recent reviews by Chen and Doolen [4] and Yu et al. [24]. The most popular LBE model is the so-called lattice BGK model, which has a single relaxation time [1, 3, 22]. However, it is well known that the lattice BGK model suffers from numerical instability and viscosity dependent boundary conditions for the velocity field, especially in under-relaxed situations [13]. It has been shown that these difficulties are a result of the BGK approximation used in the collision process and are not intrinsic to the LBE method [8, 10]. Furthermore, the multiple-relaxation-time (MRT) LBE method, or the generalized LBE method [5, 6, 8–10, 17, 19], can mitigate or overcome these difficulties.

The overall goal of this work is to compare the accuracy of LBE model9s for the solution of model problems applicable to porous medium systems in general. The specific objectives of this work are: (1) to implement a standard BGK-LBE and a MRT-LBE model; (2) to examine boundary conditions to approximate solid-fluid phase boundaries; and (3) to compare quantitatively the set of LBE models for model problems.

The remaining part of this paper is organized as follows: §2 briefly discusses the three dimensional MRT-LBE model with 19 velocities (D3Q19 model) and fluid-solid boundary condition approximations; §3 presents the numerical results for three-dimensional Poiseuille flow, and flow through a periodic simple cubic (SC) array of spheres of equal radius; and §4 concludes the paper.

2. MULTIPLE-RELAXATION-TIME LBE MODEL

2.1. D3Q19 MRT-LBE Model

There are three components in any LBE model. The first component is a discrete phase space consisting of a regular lattice space $\delta_x \mathbb{Z}^d$ with a lattice constant δ_x in d dimensions and a finite set of highly symmetric discrete velocities $\{e_i|i=0,1,\ldots,N\}$ connecting each lattice node $\boldsymbol{x}_k \in \delta_x \mathbb{Z}^d$ to its neighbors, and the corresponding set of velocity distribution functions $\{f_i|i=0,1,\ldots,N\}$ defined on each node of the lattice. The second component is a collision matrix S and (N+1) equilibrium distribution functions $\{f_i^{(eq)}|i=0,1,\ldots,N\}$. The equilibrium distribution functions are functions of the local conserved quantities. This is the most crucial component of the LBE method and it is related to the kinetic theory. The third component is an evolution equation in discrete time $t_n \in \delta_t \mathbb{N}$, where time step δ_t is set equal to unity, as is the lattice spacing $(\delta_x = \delta_t = 1)$:

$$\mathbf{f}(\boldsymbol{x}_k + \boldsymbol{e}_i \delta_x, t_n + \delta_t) - \mathbf{f}(\boldsymbol{x}_k, t_n) = \mathsf{M}^{-1} \widehat{\mathsf{S}} \left[\mathbf{m}^{(\mathrm{eq})}(\boldsymbol{x}_k, t_n) - \mathbf{m}(\boldsymbol{x}_k, t_n) \right] + \mathbf{F}, \tag{1}$$

where \mathbf{f} , $\mathbf{m}^{(eq)}$, \mathbf{m} , and \mathbf{F} are B-dimensional vectors (B = N + 1 or N for models with or without zero velocity particles, respectively),

$$\mathbf{f}(\boldsymbol{x}_{k}, t_{n}) := (f_{0}(\boldsymbol{x}_{k}, t_{n}), f_{1}(\boldsymbol{x}_{k}, t_{n}), \dots, f_{N}(\boldsymbol{x}_{k}, t_{n}))^{\mathsf{T}}, \mathbf{m}^{(\mathrm{eq})}(\boldsymbol{x}_{k}, t_{n}) := (m_{0}^{(\mathrm{eq})}(\boldsymbol{x}_{k}, t_{n}), m_{1}^{(\mathrm{eq})}(\boldsymbol{x}_{k}, t_{n}), \dots, m_{N}^{(\mathrm{eq})}(\boldsymbol{x}_{k}, t_{n}))^{\mathsf{T}}, \mathbf{m}(\boldsymbol{x}_{k}, t_{n}) := (m_{0}(\boldsymbol{x}_{k}, t_{n}), m_{1}(\boldsymbol{x}_{k}, t_{n}), \dots, m_{N}(\boldsymbol{x}_{k}, t_{n}))^{\mathsf{T}}, \mathbf{F}(\boldsymbol{x}_{k}, t_{n}) := (F_{0}(\boldsymbol{x}_{k}, t_{n}), F_{1}(\boldsymbol{x}_{k}, t_{n}), \dots, F_{N}(\boldsymbol{x}_{k}, t_{n}))^{\mathsf{T}},$$

where T denotes the transpose operator (we always assume that $e_0 \equiv \mathbf{0}$), \mathbf{F} represents the external forcing in the system, and the relaxation matrix $\hat{\mathbf{S}}$ is a diagonal matrix in this setting. The transformation matrix M relates the distribution functions represented by $\mathbf{f} \in \mathbb{V} = \mathbb{R}^B$ to their moments represented by $\mathbf{m} \in \mathbb{M} = \mathbb{R}^B$ as

$$\mathbf{m} = \mathsf{M} \cdot \mathbf{f}, \qquad \mathbf{f} = \mathsf{M}^{-1} \cdot \mathbf{m}. \tag{2}$$

The transformation matrix M, of which the matrix elements are chosen to be integers, is constructed so that $M \cdot M^T$ is a diagonal matrix.

We use the 19-velocity model in three dimensions, i.e., the D3Q19 model (here DdQq denotes the model with q velocities in d dimensions). The discrete velocities are

$$e_{i} = \begin{cases} (0, 0, 0), & i = 0, \\ (\pm 1, 0, 0), (0, \pm 1, 0), (0, 0, \pm 1), & i = 1 - 6, \\ (\pm 1, \pm 1, 0), (0, \pm 1, \pm 1), (\pm 1, 0, \pm 1), & i = 7 - 18. \end{cases}$$
(3)

The corresponding 19 moments are

$$\mathbf{m} := (\rho, e, \varepsilon, j_x, q_x, j_y, q_y, j_z, q_z, 3p_{xx}, 3\pi_{xx}, p_{ww}, \pi_{ww}, p_{xy}, p_{yz}, p_{xz}, m_x, m_y, m_z)^{\mathsf{T}}$$
$$= (m_0, m_1, \dots, m_{18})^{\mathsf{T}},$$

among which, only the density ρ and momentum $\mathbf{j} := (j_x, j_y, j_z)$ are conserved quantities for athermal fluids, and the rest are non-conserved ones. The equilibria for the non-conserved moments are [6]

$$e^{(\text{eq})} = -11\rho + \frac{19}{\rho_0} \mathbf{j} \cdot \mathbf{j} = -11\rho + \frac{19}{\rho_0} (j_x^2 + j_y^2 + j_z^2), \tag{4a}$$

$$\varepsilon^{(\text{eq})} = 3 \rho - \frac{11}{2\rho_0} \mathbf{j} \cdot \mathbf{j}, \tag{4b}$$

$$q_x^{(eq)} = -\frac{2}{3}j_x, q_y^{(eq)} = -\frac{2}{3}j_y, q_z^{(eq)} = -\frac{2}{3}j_z,$$
 (4c)

$$p_{xx}^{(eq)} = \frac{1}{3\rho_0} \left[2j_x^2 - (j_y^2 + j_z^2) \right], \qquad p_{ww}^{(eq)} = \frac{1}{\rho_0} \left[j_y^2 - j_z^2 \right],$$
 (4d)

$$p_{xy}^{(eq)} = \frac{1}{\rho_0} j_x j_y, \qquad p_{yz}^{(eq)} = \frac{1}{\rho_0} j_y j_z, \qquad p_{xz}^{(eq)} = \frac{1}{\rho_0} j_x j_z,$$
 (4e)

$$\pi_{xx}^{(eq)} = -\frac{1}{2}p_{xx}^{(eq)}, \qquad \pi_{ww}^{(eq)} = -\frac{1}{2}p_{ww}^{(eq)},$$
(4f)

$$m_x^{\text{(eq)}} = m_y^{\text{(eq)}} = m_z^{\text{(eq)}} = 0,$$
 (4g)

where ρ_0 is the (constant) mean density in the system (usually set to 1), the relaxation matrix is diagonal and is given by

$$\widehat{\mathsf{S}} = \operatorname{diag}(0, s_1, s_2, 0, s_4, 0, s_4, 0, s_4, s_9, s_{10}, s_9, s_{10}, s_{13}, s_{13}, s_{13}, s_{16}, s_{16}, s_{16})$$

$$= \operatorname{diag}(0, s_e, s_\varepsilon, 0, s_q, 0, s_q, 0, s_q, s_\nu, s_\pi, s_\nu, s_\pi, s_\nu, s_\nu, s_\nu, s_m, s_m, s_m), \tag{5}$$

and the transformation matrix M is chosen following d'Humières et al. [6]:

The speed of sound of the model is $c_s = 1/\sqrt{3}$ and the viscosity is

$$\nu = \frac{1}{3} \left(\frac{1}{s_{\nu}} - \frac{1}{2} \right). \tag{6}$$

With the above equilibria of Eqs. (4), if all the relaxation rates, $\{s_i|i=0,\cdots,18\}$, are set to be a single value $\omega=1/\tau$, i.e., $S=\omega I$, where I is the identity matrix, then the model reduces to the corresponding BGK-LBE model with the following equilibrium distribution functions [13]:

$$f_i^{\text{(eq)}} = w_i \left\{ \rho + \rho_0 \left(\boldsymbol{e}_i \cdot \boldsymbol{u} + \frac{3}{2} (\boldsymbol{e}_i \cdot \boldsymbol{u})^2 - \frac{1}{2} \boldsymbol{u} \cdot \boldsymbol{u} \right) \right\}, \tag{7}$$

where $w_0 = 1/3$, $w_i = 1/18$ for i = 1 - 6, and $w_i = 1/36$ for i = 7 - 18.

In the LBE simulations, the body force \mathbf{F} is implemented such that $\mathbf{j}' = \mathbf{j} + \mathbf{F}/2$ (or $\mathbf{u}' = \mathbf{u} + \mathbf{F}/2$) is used instead of \mathbf{j} (or \mathbf{u}) in the nonlinear terms of the equilibria [10, 19]. More detailed discussions of the MRT-LBE method are available in the literature [5, 6, 8–10, 17].

2.2. Boundary Conditions

In the LBE method, no-slip velocity boundary conditions are usually approximated using the standard bounce-back (SBB) method, which mimic the phenomenon that a particle reflects its momentum in some way when colliding with a solid surface. The SBB boundary conditions work well for boundaries consisting of flat surfaces aligned with the underlying lattice structure. For curved surfaces, a zig-zag approximation is used, and it is inaccurate especially if the resolution is coarse. For the lattice BGK model, the actual position of a boundary is viscosity dependent when the SBB boundary conditions are applied. This problem is particularly severe in under-relaxed situations, i.e., when $\tau > 1$. This problem can be easily solved by using the MRT-LBE model. In the D3Q15 MRT-LBE model, the relaxation rate for the "energy flux" mode, s_q , is chosen as the following [8, 10]:

$$s_q = 8 \frac{(2 - s_\nu)}{(8 - s_\nu)}. (8)$$

For Poiseuille flow, when the boundaries are parallel to the lattice lines, the position at which $\mathbf{u} = \mathbf{0}$ is fixed at one half lattice spacing beyond the last fluid node [2, 8–10].

To accurately represent curved boundaries, interpolations can be used. In the MRT-LBE method, bounce-back boundary conditions with interpolations can ensure accurate representation of curved boundaries in general [2, 18]. A drawback due to interpolations is that the local mass is no long conserved at locations where interpolations are applied. However, an accurate and efficient implementation of the fluid-solid boundary conditions is crucial in porous medium flow simulations with limited spatial resolution, because applying fine enough discretization of pore geometries to adequately resolve the flow with a zig-zag approximation is often computationally impractical. We will investigate a linearly interpolated bounce-back (LIBB) boundary conditions with the D3Q19 model.

3. NUMERICAL RESULTS

3.1. Poiseuille flow

We first study the case of Poiseuille flow between two parallel plates, for which the analytic solution exists. Poiseuille flow is a common test problem used in the study of LBE methods [8–10, 13] and is applicable directly to certain porous medium systems, such as fractured media. A uniform force was applied along the x-direction, by setting

$$F_i = 3w_i \rho \left(\boldsymbol{e}_i \cdot \hat{\boldsymbol{x}} \right) g, \tag{9}$$

where \hat{x} is the unit vector along x-axis, and g is the forcing magnitude. In the simulations, we fixed $g = 1.0 \times 10^{-5}$ in lattice units. We applied no-slip boundary conditions at the two plates located at the first and the eighth layers in the y-direction. Periodic boundary conditions were applied in both the stream-wise (x) and the span-wise (z) directions. The analytic solution for the velocity with a half channel height h is

$$u_x = \frac{g}{2\nu}(h^2 - y^2), \qquad |y| \le h.$$
 (10)

The system size is $N_x \times N_y \times N_z = 8 \times 8 \times 8$. With six fluid nodes between the two plates, the channel width 2h should be equal to six lattice spacings, if the no-slip boundary

conditions are satisfied exactly at one half lattice node beyond the last fluid node. For the D3Q15 MRT-LBE model, this can be accomplished by using the relaxation rate for the energy flux mode s_q , given by Eqn. (8) [8, 10]. However, for the D3Q19 model, there is an additional relaxation rate s_m that affects the position of the boundary.

Because the nonlinear advection term $\boldsymbol{u} \cdot \nabla \boldsymbol{u}$ vanishes for Poiseuille flow, we can use the *linear* LBE scheme to simulate this flow by eliminating all the nonlinear terms (in terms of \boldsymbol{j} or \boldsymbol{u}) in the equilibria of Eqs. (4) for the moments, or equivalently in the the equilibria of Eqn. (7) for the distribution functions. Effectively, the linear LBE scheme simulates Stoke flow.

For Poiseuille flow, the normalized flow rate is a constant:

$$\overline{Q} = \frac{3}{4hU_{\text{max}}} \int_{-h}^{+h} u_x(y)dy = 1,$$
 (11)

where $u_x(y)$ is given by Eqn. (10) and $U_{\text{max}} = gh^2/2\nu$. In order to obtain a constant \overline{Q} in the simulations with a given channel width 2h, it is crucial to have precise knowledge and control of the position at which the no-slip boundary conditions are satisfied. Thus Poiseuille flow was used to test the boundary conditions in the D3Q19 LBE models.

In addition to the relaxation rate s_{ν} , which determines the viscosity, there are five other relaxation rates that are adjustable parameters: s_e , s_{ε} , s_q , s_{π} and s_m . With a fixed value of the viscosity, we chose three sets of relaxation rates shown in Table 1, and compared the results with the BGK-LBE results.

Table 1 Relaxation rates for Poiseuille flow simulations. $s_q(s_{\nu})$ is given by Eqn. (8).

	s_e	$s_{arepsilon}$	s_q	s_{π}	s_m
MRT-1	$s_q(s_{\nu})$	$s_q(s_{\nu})$	$s_q(s_{\nu})$	$s_q(s_{\nu})$	$s_q(s_{\nu})$
MRT-2	1.98	1.98	$s_q(s_{\nu})$	1.98	$s_q(s_{\nu})$
MRT-3	$s_q(s_{\nu})$	$s_q(s_{\nu})$	$s_q(s_{\nu})$	$s_q(s_{\nu})$	1.98

We applied linear regression to fit the parabolic profile of $u_x(y)$ obtained by the simulations to obtain the values of h^* and ν^* , which in turn determines the values of s_{ν}^* in the MRT-LBE scheme and $\tau^* = 1/s_{\nu}^*$ in the BGK-LBE scheme. With the values of s_{ν}^* (or τ^*) and h^* obtained with linear regression, we computed the error of the velocity profile using the L^2 -norm

$$E_2(u) = \sqrt{\frac{\sum_y |u_x(y) - u_x^*(y)|^2}{\sum_y |u_x^*|^2}},$$
(12)

where $u_x(y)$ and $u_x^*(y)$ are the numerical and analytical solutions, respectively. The results are tabulated in Table 2.

The results for the value of s_{ν}^* (or $\tau^* = 1/s_{\nu}^*$) obtained by linear regression agree very well with the input values (at least 5 figures), despite the fact that there may be corrections

Table 2 Comparison of the relative error $E_2(u)$ in the flow velocity profile and the half-channel width h^* , using the MRT model with various parameters given in Table 1 and the BGK model. The half-channel width h is supposed to be 3 lattice units.

$\tau = 1/s_{\nu}$	model	$E_2(u)$	h^*
	MRT-1	5.6364×10^{-9}	3.0000
0.6	MRT-2	5.6363×10^{-9}	3.0000
0.0	MRT-3	5.3915×10^{-9}	2.9687
	BGK		2.9630
	MRT-1	3.1775×10^{-10}	3.0000
0.8	MRT-2	3.1777×10^{-10}	3.0000
0.0	MRT-3	7.3602×10^{-10}	2.9688
	BGK	8.3723×10^{-10}	2.9783
	MRT-1	9.0771×10^{-11}	3.0000
1.0	MRT-2	9.0854×10^{-11}	3.0000
1.0	MRT-3	8.3499×10^{-11}	2.9690
	BGK	1.7455×10^{-12}	3.0139
	MRT-1	1.9050×10^{-12}	3.0000
1.5	MRT-2	1.9173×10^{-12}	3.0000
	MRT-3	8.4391×10^{-14}	2.9694
	BGK	2.6370×10^{-13}	3.1754
	MRT-1	1.9578×10^{-12}	3.0000
2.0	MRT-2	1.9365×10^{-12}	3.0000
- ··	MRT-3	2.0564×10^{-12}	2.9699
	BGK	2.4058×10^{-13}	3.4278

for such a small channel size [17]. Thus the values of s_{ν}^{*} (or τ^{*}) are not given in Table 2. The results in Table 2 show that the velocity profile $u_{x}(y)$ is a parabola independent of the models used, as indicated by $E_{2}(u)$. The only difference is the effect of the viscosity ν on the numerical half channel width h^{*} . For the MRT model, it is clear that the "effective" channel width $2h^{*}$ does not depend on the viscosity ν , while for the BGK model, h^{*} strongly depends on ν , particularly when it is under-relaxed: the maximum deviation of h^{*} is about 15.0% when $\tau=2.0$, which corresponds to more than a 40% error in the velocity field compared to the analytic solution for the expected values of s_{ν} and h. We also observe that the relaxation rate s_{m} affects the value of h^{*} , while s_{e} , s_{q} , and s_{π} do not, as indicated by the results correspondence of MRT-2 and MRT-3. Nevertheless, this effect is of high order and controllable (the variation of h^{*} is about 1.0%).

3.2. Flow through a simple cubic array of spheres

We next considered the case of flow through an idealized porous medium, i.e., a periodic simple cubic (SC) array of spheres of equal radius a, as depicted in Fig. 1. The theoretical

fluid permeability κ^* for a viscous flow past an array of spheres is [23]

$$\kappa^* = \frac{1}{6\pi a d^*}, \qquad d^* = \frac{6\pi a \rho \nu u_{\rm d}}{F_D},\tag{13}$$

where u_d is the Darcy velocity along the flow direction, and F_D is the drag force. The inverse of the dimensionless drag, d^* , is purely determined by the geometric characteristics of the sphere array, and it can be represented by a function of the solid volume fraction c as a series expansion [23]:

$$d^* = \sum_{n=0}^{30} q_n \chi^n, \qquad \chi = \left(\frac{c}{c_{\text{max}}}\right)^{1/3}, \qquad c = \frac{4\pi a^3}{3L^3}, \qquad c_{\text{max}} = \frac{\pi}{6}, \tag{14}$$

where L is the length of the cube, and the coefficient q_n can be obtained analytically [23]. We measure the fluid permeability κ according to Darcy's law at low Reynolds number:

$$u_{\rm d} = -\frac{\kappa}{\rho \nu} \left(\nabla p - \rho g \right), \tag{15}$$

where Darcy velocity u_d is obtained as the volume averaged velocity over the system [21].

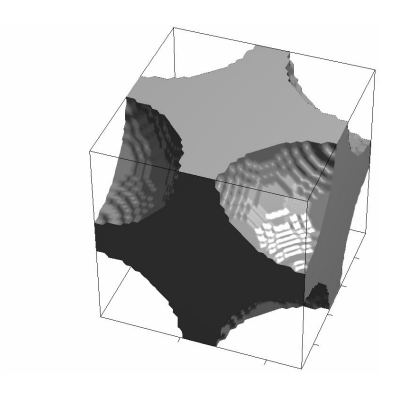


Figure 1. A typical pore geometry of a SC array of spheres ($\chi = 0.8$). Gray and white area depict fluid and solid regions, respectively.

In the simulations, we use the *linear* lattice Boltzmann equation as in the previous case, for both the MRT and BGK schemes [2, 18]. Hereinafter notations MRT-LIBB, MRT-SBB, and BGK-SBB are used to denote the MRT scheme with linearly interpolated bounce-back boundary conditions (BC), the MRT scheme with the standard bounce-back BCs, and the lattice BGK scheme with the standard bounce-back BCs, respectively. Various system sizes N^3 are used in our simulations. Obviously, the radius is $a = \chi N/2$.

Table 3 shows the relative errors of κ between linear LB simulations and theoretical predictions of Stokes flow through the SC sphere arrays, given in Eqs. (13) and (14), with $\chi = 0.7$ and 0.95, and with system sizes $N^3 = 32^3$ and 64^3 . In the MRT scheme, we

Table 3 The relative errors of κ for flow through a periodic SC array of spheres, using the MRT-LIBB, MRT-SBB and BGK-SBB schemes.

V	$1/s_{\nu}$	MRT-LIBB		MRT-SBB		BGK-SBB	
χ	$1/3\nu$	32^{3}	64^{3}	32^{3}	64^{3}	32^{3}	64^{3}
	0.6	0.39%	0.16%	-3.59%	-1.99%	-6.96%	-3.57%
	0.8	1.10%	0.32%	-2.78%	-1.38%	-3.88%	-1.79%
0.7	1.0	1.59%	0.45%	-2.36%	-1.19%	-1.69%	0.93%
	1.5	2.53%	0.70%	-1.90%	-0.96%	4.37%	1.15%
	2.0	3.32%	0.93%	-1.72%	-0.34%	11.9%	3.59%
	0.6	-0.78%	0.09%	-7.72%	-1.92%	-12.9%	-4.08%
	0.8	0.85%	0.50%	-6.33%	-1.34%	-8.35%	-2.11%
0.95	1.0	1.94%	0.76%	-5.67%	-1.06%	-4.60%	0.67%
	1.5	4.05%	1.29%	-4.95%	-0.70%	5.37%	2.73%
	2.0	5.83%	1.74%	-4.67%	-0.56%	17.17%	6.77%

use the parameters given by the set MRT-1 in Table 1. The results clearly show that the values of κ obtained by the MRT schemes are much less dependent on viscosity than those obtained by the BGK-SBB counterparts, and in all cases the results obtained with the MRT schemes are consistently better than those obtained with the BGK-SBB scheme. We also note that in general linear interpolation improves the simulation accuracy. The improvement is particularly significant (by an order of magnitude) for over-relaxation ($\tau = 1/s_{\nu} < 1$), where more iteration time is required to reach a steady state than in under-relaxations ($\tau > 1$).

Table 4 The relative errors of the permeability κ for a periodic SC array of spheres with a grid resolution of 32^3 using the MRT-LIBB and MRT-SBB schemes, where ϕ is the porosity.

χ	ϕ	MRT-LIBB	MRT-SBB
0.5	0.93	-0.36%	-4.31%
0.6	0.89	0.39%	-3.59%
0.7	0.82	0.69%	-1.59%
0.8	0.73	-0.01%	-3.79%
0.9	0.62	-0.12%	-6.35%
0.95	0.55	-0.65%	-7.72%

To further demonstrate the effect of interpolation schemes, we performed the full (non-linear) MRT-LBE simulations, which recovers the Navier-Stokes equations (as opposed to the Stokes equation), for the periodic SC arrays of spheres with various radii and a fixed system size 32^3 . All the simulations were performed at Reynolds numbers Re < 0.01 to ensure that the flow was in the Stokes regime. We fixed the value of τ at 0.6. Table 4

shows the relative error of the permeability κ with respect to the theoretical predictions, using both the MRT-LIBB and MRT-SBB schemes. Clearly, interpolations significantly improved the accuracy for wide range of χ .

We also investigated discretization effects for both the MRT-LIBB and MRT-SBB methods. The results shown in Figure 2 confirm the improvement due to the linear interpolation method. Furthermore, we find that the interpolation scheme converges faster to the theoretical solution for the MRT-LIBB scheme than for the MRT-SBB scheme. This is crucial in porous medium flow simulations, because computational limitations are commonplace for standard problems of concern.

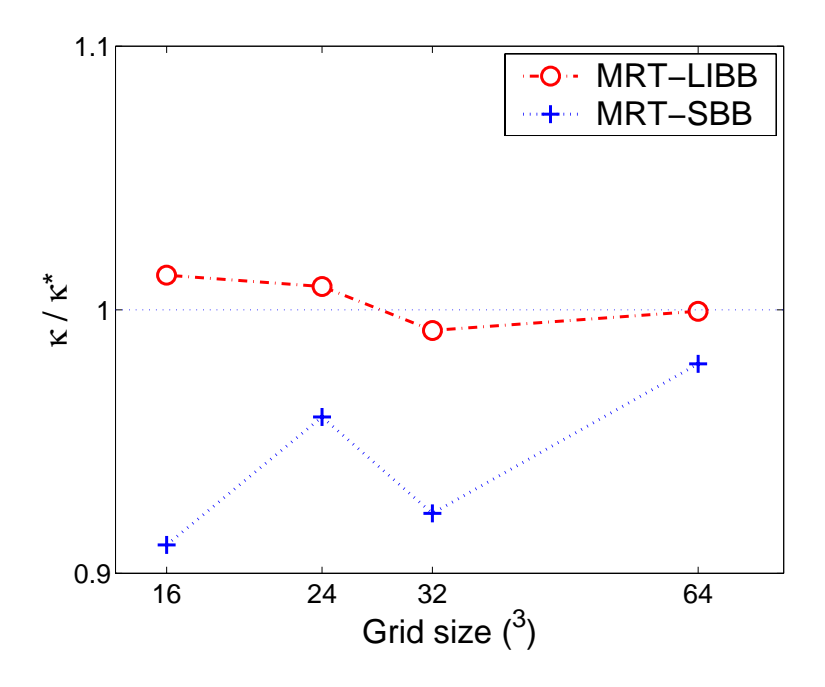


Figure 2. The normalized permeability κ/κ^* (κ^* is given by Eqn. (13)) as a function of grid resolution for the SC array of spheres with $\chi=0.95$, simulated by the MRT-SBB and MRT-LIBB schemes.

4. CONCLUSION

In this work we observed that the MRT models significantly reduce the viscosity dependence of permeability in LBE porous medium simulations compared to their BGK-LBE counterparts. The reason is that in the MRT model the location where the flow boundary conditions are satisfied can be essentially viscosity independent, which is impossible for the BGK-LBE model. Our results for both Poiseuille flow and flow through a SC array of spheres clearly demonstrate the advantages of the MRT models over their lattice BGK counterparts.

We also show that LIBB scheme can significantly improve the accuracy of simulations, provided that sufficient resolution is given to apply the interpolations. The improvement due to interpolations is particularly significant with over-relaxation ($\tau < 1$), and it is more significant for Navier-Stokes flows than for Stokes flows. In addition, we show that the LIBB scheme converges more rapidly than the SBB scheme and provides more accurate results for a given grid resolution. We find that the effect due to interpolations on mass conservation is negligible in our simulations.

We also observed the effect of the relaxation rate s_m on the boundary location. This effect is relatively small, and analysis is left for future work.

ACKNOWLEDGEMENT

LSL is grateful to Drs. I. Ginzburg and D. d'Humières for providing ref. [10] before its publication, and to Dr. P. Lallemand for insightful discussions. This work was supported in part by National Science Foundation (NSF) grant DMS-0327896, NSF grant DMS-0112069 to the Statistical and Applied Mathematical Sciences Institute, and grant P42 ES05948 from the National Institute of Environmental Health Sciences.

REFERENCES

- 1. P. Bhatnagar, E. Gross, and M. Krook. A model for collsion processes in gases. *Phys. Rev.*, 94:511–525, 1954.
- 2. M. Bouzidi, M. Firdaouss, and P. Lallemand. Momentum transfer of a Boltzmann-lattice fluid with boundaries. *Phys. Fluids*, 13:3452–3459, 2001.
- 3. H. Chen, S. Chen, and W. H. Matthaeus. Recovery of the Navier-Stokes equations using a lattice-gas Boltzmann methods. *Phys. Rev. A*, 45:5339–5342, 1992.
- 4. S. Chen and G. D. Doolen. Lattice Boltzmann method for fluid flows. *Annu. Rev. Fluid Mech.*, 30:329–364, 1998.
- D. d'Humières. Generalized lattice Boltzmann equations. Prog. Astonat. Aeronaut, 159:450–458, 1992.
- 6. D. d'Humières, I. Ginzburg, M. Krafczyk, P. Lallemand, and L.-S. Luo. Multiple-relaxation-time lattice Boltzmann models in three dimensions. *Philos. Trans. R. Soc. Lond. A*, 360:437–451, 2002.
- 7. U. Frisch, B. Hasslacher, and Y. Pomeau. Lattice-gas automata for the Navier-Stokes equation. *Phys. Rev. Lett.*, 56:1505–1507, 1986.
- 8. I. Ginzbourg and P. M. Adler. Boundary flow condition analysis for the three-dimensional lattice Boltzmann model. *J. Phys. II*, 4:191–214, 1994.
- 9. I. Ginzburg and D. d'Humières. Local second-order boundary methods for lattice Boltzmann models. *J. Stat. Phys.*, 88:927, 1997.
- 10. I. Ginzburg and D. d'Humières. Multireflection boundary conditions for lattice Boltzmann models. *Phys. Rev. E*, 68:066614:1–30, 2003.
- 11. X. He and L.-S. Luo. A priori derivation of the lattice Boltzmann equation. *Phys. Rev. E*, 55:R6333–R6336, 1997.
- 12. X. He and L.-S. Luo. Theory of lattice Boltzmann method: From the Boltzmann equation to the lattice Boltzmann equation. *Phys. Rev. E*, 56:6811–6817, 1997.
- 13. X. He, Q. Zou, L.-S. Luo, and M. Dembo. Analytic solutions and analysis on non-slip

- boundary condition for the lattice Boltzmann BGK model. J. Stat. Phys., 87:115–136, 1997.
- 14. M. Junk and A. Klar. Discretizations for the incompressible Navier-Stokes equations based on the lattice Boltzmann method. SIAM J. Sci. Comput., 22:1–19, 2000.
- 15. M. Junk, A. Klar, and L.-S. Luo. Asymptotic analysis of the lattice Boltzmann equation. *in review*, J. Computat. Phys., 2004.
- 16. M. Junk and W.-A. Yong. Rigorous Navier-Stokes limit of the lattice Boltzmann equation. *Asymp. Anal.*, 35:165–185, 2003.
- 17. P. Lallemand and L.-S. Luo. Theory of the lattice Boltzmann method: Dispersion, dissipation, isotropy, Galilean invariance, and stability. *Phys. Rev. E*, 61(6):6546–6562, 2000.
- 18. P. Lallemand and L.-S. Luo. Lattice Boltzmann method for moving boundaries. *J. Computat. Phys.*, 184:406–421, 2003.
- 19. P. Lallemand and L.-S. Luo. Theory of the lattice Boltzmann method: Acoustic and thermal properties in two and three dimensions. *Phys. Rev. E*, 68:036706, 2003.
- 20. G. R. McNamara and G. Zanetti. Use of the Boltzmann equation to simulate lattice-gas automata. *Phys. Rev. Lett.*, 61(20):2332–2335, 1988.
- 21. C. Pan, M. Hilpert, and C. T. Miller. Pore-scale modeling of saturated permeabilities in random sphere packings. *Phys. Rev. E*, 64(6):article number 066702, 2001.
- 22. Y. H. Qian, D. d'Humières, and P. Lallemand. Lattice BGK models for Navier-Stokes equation. *Europhys. Lett.*, 17(6):479–484, 1992.
- 23. A. S. Sangani and A. Acrivos. Slow flow through a periodic array of spheres. *Int. J. Multiphase Flow*, 8(4):343–360, 1982.
- 24. D. Yu, R. Mei, L.-S. Luo, and W. Shyy. Viscous flow computations with the method of lattice Boltzmann equation. *Prog. Aerospace Sci.*, 39:329–367, 2003.